# In Vivo Spin-Label Murine Pharmacodynamics Using Low-Frequency Electron Paramagnetic Resonance Imaging

Howard J. Halpern,* Miroslav Peric,* Cheng Yu,* Eugene D. Barth,* G. V. R. Chandramouli,* Marvin W. Makinen,# and Gerald M. Rosen§

*Department of Radiation and Cellular Oncology, University of Chicago, Chicago, Illinois 60637 USA, #Department of Biochemistry and Molecular Biology, University of Chicago, Chicago, Illinois 60637 USA, and §Department of Pharmaceutical Sciences, University of Maryland School of Pharmacy, Baltimore, Maryland 21201 USA

ABSTRACT A novel, very-low-frequency electron paramagnetic resonance (EPR) technique is used to image the distribution of several nitroxides with distinct pharmacologic compartment affinities in the abdomens of living mice. Image acquisition is sufficiently rapid to allow a time sequence of the distribution for each compound. The spectra and concentrations of these nitroxides are imaged with the use of spectral-spatial imaging to distinguish a single spatial dimension. Liver and bladder of the mouse anatomy are distinguished by this technique. After an intraperitoneal injection of the spin-label probes, a shift in the distribution of the compounds from the upper abdomen (primarily liver) to the lower abdomen (primarily bladder) is observed. The time dependence of the shift in regional distribution depends on the structural properties of the side chain attached to the spin label. These results indicate that this application of in vivo electron paramagnetic resonance imaging will provide a new method of magnetic resonance imaging for determination of pharmacodynamics in the body of an intact animal.

## INTRODUCTION

One of the major challenges in pharmacologic studies is the determination of the distribution and metabolism of a drug in an intact animal. To this end radioisotopes are commonly used tools, yielding quantitative measures of the organ distribution of a drug (Antar, 1990; Kung, 1990; Stocklin, 1992). Noninvasive imaging permits the time sequence monitoring of the distribution of a drug (Antar, 1990; Kung, 1990; Reba, 1993; Stocklin, 1992). However, radio nuclear images may suffer from limited spatial resolution, making it difficult to apply to laboratory animal models such as mice. In addition, radio-labeled compounds have short shelf lives and require specialized production instrumentation (Reba, 1993), both of which increase experimental costs. They may also be limited by the stability of the drug–radio nuclide bond with consequent nonspecific tissue uptake of activity (Stocklin, 1992). Tracers requiring metal chelates may sufficiently alter the molecular weight, the conformation, the shape, or the pharmacologic properties of the drug to render the study of low relevance (Stocklin, 1992). Finally, there are concerns about patient exposure to the radioactive tracer (Loevinger and Berman, 1976, 1968).

Paramagnetic species can be detected directly by electron paramagnetic resonance (EPR) imaging (Berliner and Fuji, 1985; Herrling et al., 1982; Lauterbur et al., 1984; Maltempo, 1986) rather by inference of their presence by their influence on the relaxation of water hydrogen nuclei, as must be done in magnetic resonance imaging. The development of imaging EPR spectroscopy (Bacic et al., 1988; Fuchs et al., 1992; Kuppusamy et al., 1994; Maltempo et al., 1987) at very low frequency (Alecci et al., 1994; Halpern et al., 1989), under which conditions stable free radicals can be detected and localized in vivo, permits determination of drug distribution and metabolism in whole animals. By using field gradients, one can localize the source of the resonant signal in small animals such as mice, and images of the spatial distribution of a paramagnetic species can be acquired rapidly enough for its time-dependent distribution to be determined (Alecci et al., 1994). Here we apply this methodology to determine the time-dependent organ distribution of nitroxides with distinct pharmacologic compartment affinity in the abdomens of C3H mice.

Although results of preliminary studies were reported earlier (Boisvert et al., 1993; Halpern et al., paper read at XVII International EPR Symposium, 1994), here we present results that demonstrate with improved evaluation of the statistical significance that the time course of the organ distribution of spin labels in a mouse can be followed by very-low-frequency EPR imaging. The mouse's major organs are distinguishable along its spinal axis, as shown in Fig. 1. The use of a single spatial dimension allows rapid image acquisition. A time sequence of images allows measurement of the time-dependent changes in the net accumulation and release of the spin-labeled compounds along the spatial dimension corresponding to the locations of the liver and the bladder after an intraperitoneal injection. Reproducible changes in the tissue compartmentation of spin-label compounds are obtained with differences corresponding to the lipophilic character of the side chain at the 3-position of the oxypyrrolidinyl and oxypyrrolinyl rings.

*Received for publication 29 January 1996 and in final form 29 March 1996.*

Address reprint requests to Dr. Howard Halpern, Department of Radiation and Cellular Oncology, University of Chicago Medical Center, MC 0085, 5841 South Maryland Avenue, Chicago, IL 60637. Tel.: 312-702-0006; Fax: 312-702-0610; E-mail: h-halpern@uchicago.edu.



0006-3495/96/07/403/07 $2.00

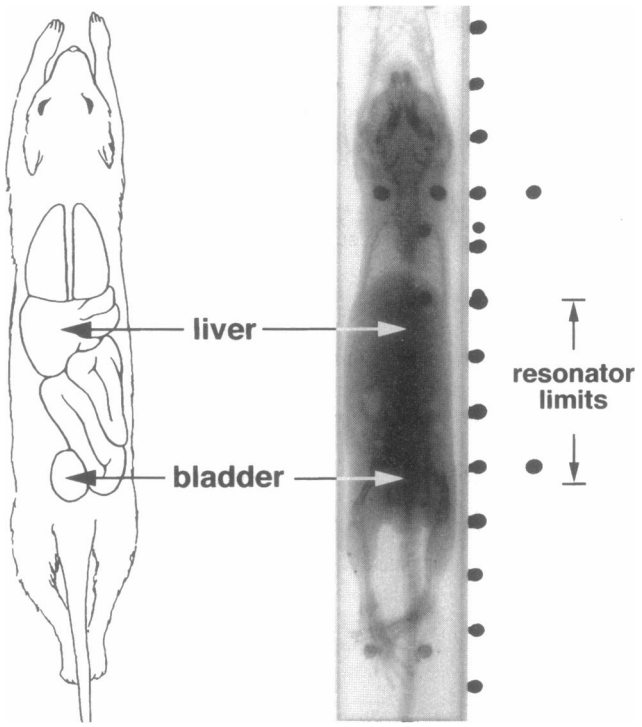


FIGURE 1 Anatomy of the mouse presented diagrammatically. The liver and the bladder are indicated. Placed next to the diagram is a supine radiograph of the mouse. The gridded dots are centimeter measuring marks. The dots not on the grid were used for animal setup and were 12 mm caudad to the scapulae for each mouse. These were used for individual mouse setup.

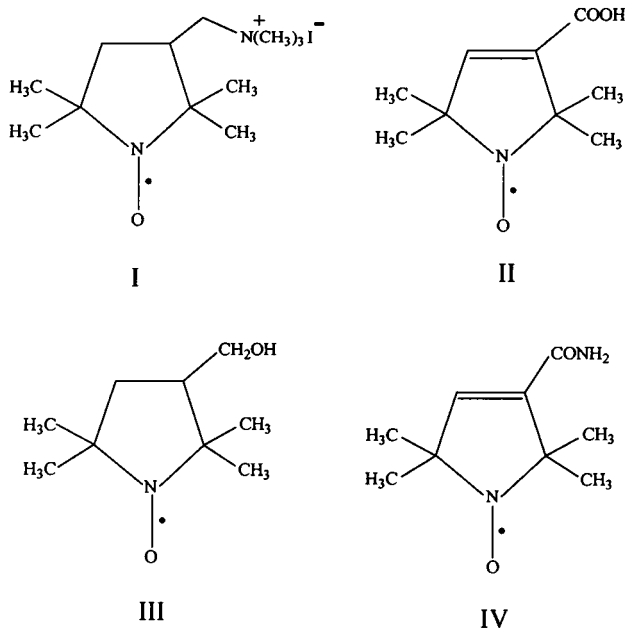


FIGURE 2 Chemical bonding structures of the four spin-label compounds used for imaging: 3-trimethylaminomethyl-2,2,5,5-tetramethyl-1-oxypyrrolidine iodide (*I*), 3-carboxy-2,2,5,5-tetramethyl-1-oxypyrroline (*II*), 3-hydroxymethyl-2,2,5,5-tetramethyl-1-oxypyrrolidine (*III*), and 3-carbamoyl-2,2,5,5-tetramethyl-1-oxypyrroline (*IV*).

The results of these studies indicate that with very-low-frequency EPR the time course of the organ distribution of spin labels can be followed. Because the technique is conveniently applied and relatively inexpensive, the results presented indicate that the method could be developed as a noninvasive technique for the study of the pharmacodynamics of the organ distribution of drugs and of their metabolism.

## METHODS

The structural formulas of the spin-label compounds used are shown in Fig. 2. The spin labels 3-trimethylaminomethyl-2,2,5,5-tetramethyl-1-oxypyrrolidine iodide (I), 3-carboxy-2,2,5,5-tetramethyl-1-oxypyrroline (II), 3-hydroxymethyl-2,2,5,5-tetramethyl-1-oxypyrrolidine (III) and 3-carbamoyl-2,2,5,5-tetramethyl-1-oxypyrroline (IV) were synthesized according to methods published by others (Rosantzev (1970), IV; Pou et al. (1995), I; and Hideg et al. (1980), II and III). For phantom measurements, spin label IV was used as the spin probe at a concentration of 200 $\mu$M in distilled water. For animal measurements the spin-labeled chemicals were dissolved in distilled water to a concentration of 30 mM (Baker, Phillipsburg, NJ) and injected as a 0.7 ml intraperitoneal (IP) bolus.

For in vivo imaging studies C3H/sed mice, 10 to 25 weeks old, were anesthetized with ketamine (45 mg/kg) and diazepam (20 mg/kg) administered IP, after which the mice were placed prone in a hemicylindrical acrylic restraint jig. The procedure was painless, but the anesthesia minimized animal motion. The mice were restrained with Elastoplast under gentle tension. Animals were treated in compliance with Federal regulations according to Public Health Service Policy A3532–01 as indicated in University of Chicago Institutional Animal Care and Use Protocol 52011. The scapulae of each mouse were palpated, and the caudad tips were marked with a nonparamagnetic marker. The position of the restraint jig with the mouse inside was adjusted to place these marks 12 mm outside the cephalad edge of a resonator 3.2 cm in length. This positioned the diaphragmatic domes at the edge of the resonator. X-ray studies of eight mice of weight 20–25 g positioned in this fashion were taken to measure the reproducibility of their positions relative to the diaphragmatic domes and the anterior superior iliac spines.

The rectal temperature was measured before and after measurement with a Physitemp thermocouple thermometer. Temperature was maintained at 36.5°C to within 1°C with radiant heating from a gooseneck lamp. The 0.7 ml of a 30 mM spin probe solution was injected IP 10 min after administration of anesthesia. No toxic reaction was observed. The restraint jig was suspended independently from the resonator to ensure mechanical decoupling. Imaging began 3–5 min after administration of the spin label.

Spectra and spectral projections for imaging were obtained with a low-frequency EPR spectrometer operating at 250 MHz (Halpern et al., 1989). At this frequency, the skin depth (37% sensitivity) is approximately 7 cm of tissue (Halpern et al., 1989; Roschmann, 1987). This frequency is far lower than that necessary for measurement deep in the tissues of a mouse. However, the use of very low frequency minimizes phase-distortion artifacts. The spectrometer consists of a lumped circuit parallel inductance and capacitance resonator, in which the single turn inductance is the sample holder. The capacitive coupling is adjustable electronically. This feature allows animal motion and microphonically induced variations in the coupling to be corrected for variations of frequencies up to several hundred hertz. The characteristics of the resonator are such that the radio frequency magnetic field ($B_1$) at an incident radiofrequency power of 100 mW and at a loaded $Q$ (quality factor) of 65 produced by the animal sample is ~0.15 G (Halpern et al., 1989). The modulation frequency was 5.12 kHz. Modulation field amplitude was 0.4 G. Data acquisition was accomplished under the control of a microcomputer. Spectral projections were obtained with 32 points per scan, 10 scans per projection. The time

constant and point acquisition time were 0.1 s, giving a projection acquisition time of just over 0.5 min. No weighting was given to high gradient scans to compensate for the lower signal-to-noise ratio.

Two-dimensional spectral-spatial images (Hayner and Jenkins, 1984; Maltempo et al., 1987, 1988) (one spectral dimension, one spatial dimension along the spinal axis of the mouse abdomen) were obtained under continuous-wave conditions. The spectral window was limited to the central feature of the EPR spectrum of these $^{14}N$-containing nitroxyl spin labels. Samples were subjected to sequences of fixed gradients, referred to as projections, during spectral acquisition. We generated 16 projections in 17 min by splaying the main field coils to give a maximum (single) gradient of 2.4 G/cm, similar to that previously described (Halpern et al., 1989). Each gradient intermixes field strength and position variables in the same way in which a planar rotation intermixes Cartesian coordinates in two dimensions for computed tomography. Images are then reconstructed by means of backprojection reconstruction. The algorithm of Hayner (Hayner and Jenkins, 1984) for incomplete angular coverage was employed. The code for this has been kindly provided by S. Eaton and G. Eaton (Maltempo et al., 1988) and was modified by us for our use. This algorithm allows the treatment of projections that are "missing" because of gradient and scan window limitations. These studies used a pseudo-object in spectral-spatial space with a length of 6 cm, a field interval of 5 G, and a Hamming filter constant of 0.5. This allows the sensitive region of the resonator (length 3.2 cm) to be encompassed fully by the image boundaries. These settings are such that a single "missing" projection at either extreme is used in the extrapolation procedure to fill the spectral-spatial space uniformly.

To understand the spatial resolution provided by the available gradients for spin labels with ~1-G linewidth, we imaged the phantom shown in Fig. 3. The phantom was divided into three axially disposed compartments with center-to-center distances of 10 mm. The end disks were filled with a 200 $\mu$M solution of spin label IV. The center disk remained empty. The phantom was imaged as described above for the mice.

## RESULTS

Fig. 3 shows the spectral-spatial image obtained with spin label IV as well as a diagram of the phantom. The 1-G linewidth of IV is virtually identical to that of the other compounds injected into the mice, providing a measure of the resolution of this technique under the gradient and EPR spectral linewidths used. Note that the smaller peak corresponds to the smaller compartment of the phantom. The end of the resonator at which the small compartment was located was the cephalad end of the resonator for animal measurements. With the compounds and gradients used, the resolution was 1 cm. With narrower spectral lines, longer acquisition times, or higher gradients, the resolution can be further extended.

Resolution of 1 cm, however, is sufficient to resolve the liver and the bladder of the mouse, whose x-ray image is shown in Fig. 4 next to a spectral-spatial image of its abdomen. To the left of the spectral-spatial image is a plot of the spectral maximum as a function of position. This spatial profile shows two distinct peaks for which the center positions differ by the same distance as do the centers of the liver and the bladder. By using the spectral maximum instead of the projected spectral intensity, we avoid modest star artifacts from the backprojection reconstruction.

Analysis of the x-ray studies of the mouse diaphragmatic domes and anterior superior iliac spines indicated a standard deviation of 2.5 mm in the positions of these structures relative to the edges of the resonator. This was significantly less than the resolution of the images presented here. For each spin label, sequences of spatial images were obtained from the spectral-spatial images. Each image was obtained in 17 min and thereby represents an average over the changing substrate spatial distribution over that time interval. We refer to the time at which the images were obtained as the time midway between start and finish of the image acquisition, or mean time of acquisition.

Although this is not evident from the displays, which are normalized to the maximum value, there is a steady reduction of the magnitude of the overall signal. Of the compounds studied, the nonspecific tissue diminution—bioreduction—of spin label I was by far the slowest. To shift the focus of this study from overall diminution of signal with time owing to bioreduction of the nitroxyl group to spatially and anatomically salient features, we plot the spatial distributions with the same maximum value.

Fig. 5 shows the time sequence of spectral-spatial images obtained from four experiments with spin label II.

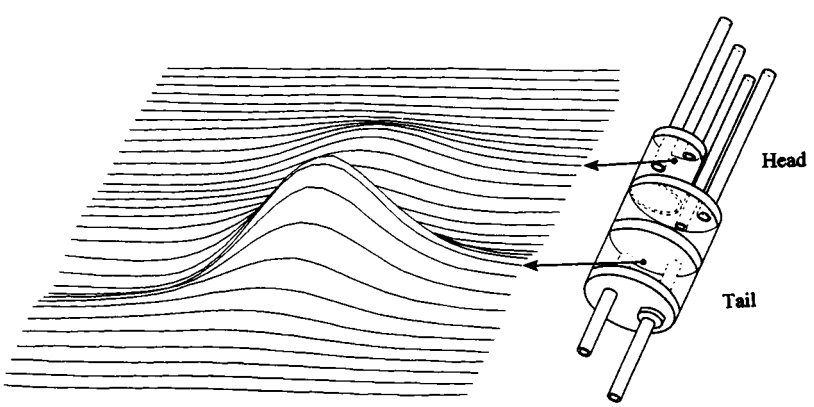


FIGURE 3 Spectral-spatial image of a phantom with compartmentalized spin label IV. The central nitrogen manifold of the nonderivative spectrum of IV with unresolved hydrogen hyperfine was included in the two-dimensional spectral-spatial image (one spatial dimension, one spectral dimension) of a phantom consisting of three compartments. The spatial direction imaged is along the axis of the cylinder. The outer compartments were filled with 200 $\mu$M spin-label IV in distilled water, and the middle compartment was left empty. The small compartment shown farthest into the page occupied the position in the resonator closest to the mouse head, the cephalad position. This is the location of the liver. The larger compartment occupied the anatomic location of the bladder.

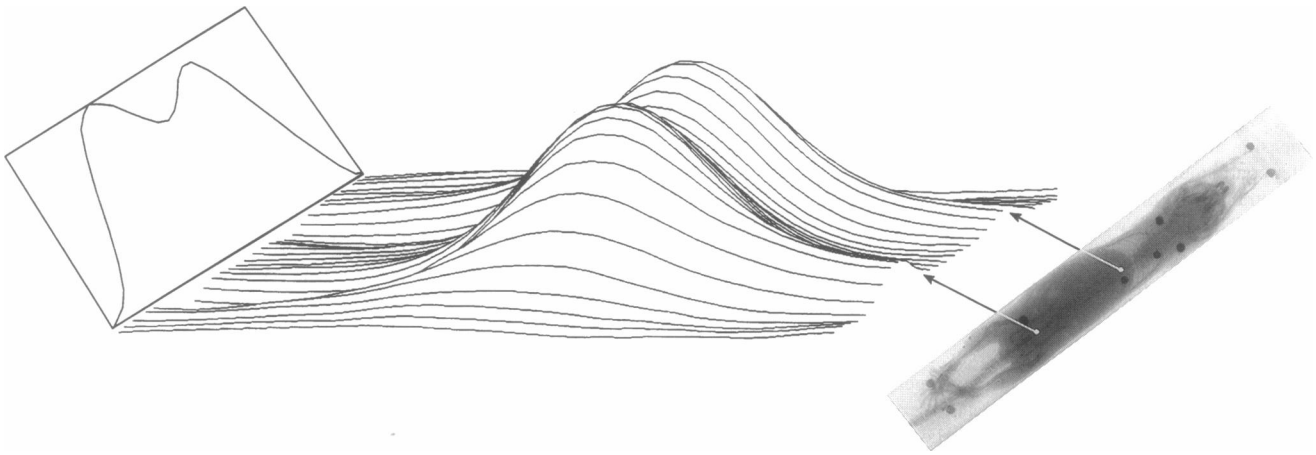

FIGURE 4 Spectral spatial image of a mouse infused with spin-label II. The mouse is oriented with its head into the page. Again, the image is restricted to the central nitrogen manifold of the nonderivative spectrum of spin label II. The image was obtained in 17 min, a mean of 89 min after IP infusion of the spin-labeled compound. Distinct peaks can be seen in the region of the liver and bladder.

The figure shows a shaded region about the line representing the mean ± SE, inclusive of the 2.5-mm positioning uncertainty. The images from different mice injected with the same compound show good consistency. Fig. 6 depicts the time-dependent changes in the distribution of spin labels I–IV superimposed to accentuate the distinctive anatomic time-distribution differences of each compound.

A number of consistencies emerge from the images. The initial spatial distribution peaks centrally. This is consistent with the IP distribution of the spin-labeled compound just after infusion. The next several spatial distributions show accumulation of the spin-labeled compound toward the cephalad side of the resonator in the region of the liver. Again this is to be expected from a compound that is absorbed through the mesenteric and omental vessels, which, in turn, feed the portal circulation. Finally, the latter spatial distributions show an accumulation of signal in the more caudad aspect of the abdomen consistent with the location of the bladder. The rate of accumulation of bladder distribution is the same for various mice injected with the same compound but varies among compounds.

For compounds I and II there is an early liver component of the distribution, seen even in the first image in the case of compound I. The liver component persists for approximately 100 min, as shown in Fig. 6. Gradually a component develops in the bladder region. The quaternary amine I was much longer lived than the carboxylic acid II.

With the methyl alcohol derivative III, the liver component of the signal diminishes rapidly relative to the bladder component. It never emerges as a distinct entity, although it is suggested in cephalad broadening of the second image relative to the first. There is a rapid development of a bladder region peak, which persists as the liver region signal diminishes. Spin label IV has an intermediate behavior between I–II and III.

## DISCUSSION

We present here a novel application of EPR spectroscopy to image the pharmacodynamics of simple spin-labeled compounds in mice. Use is made of the technique at very low frequencies, probably lower than is necessary for clear signal from such small animals. Moreover, the small size of the mouse as a sample makes these measurements more difficult than for a larger animal. As such it provides a proof of principle for use, without change in frequency, in larger animal subjects.

The image used here is simplified because it is one dimensional and is collected with low field gradients. Alecci and co-workers have used two-dimensional imaging in the rat to provide imaging pharmacodynamics of a single compound, a carboxylic acid, in the rat (Alecci et al., 1994). Their images were of higher resolution than those presented here. However, for analysis, they also take advantage of the one-dimensional distribution of rodent organ systems to derive nitroxide distributions similar to those presented here. The generalization to a three-dimensional system is straightforward. The implementation of such a system is under way in our laboratory. It has been pursued at higher frequencies by Kuppusamy and co-workers (Kuppusamy et al., 1994) for images derived from a cardiac organ preparation. The spatial resolution of the system can be improved by an order of magnitude with higher gradients. Another half-order-of-magnitude improvement could be gained with deuterated spin-labeled analogs, the spectra of which exhibit fourfold narrower spectral lines than the lines of the spin labels used here (Halpern et al., 1993). Further narrowing of the spectral line has been reported for solid-state, exchange-narrowed paramagnetic probes (Liu et al., 1993). Although these means of resolution enhancement are probably optimal in a three-dimensional system, the simple one-dimensional image form presented here provides a means for useful and reasonably rapid data acquisition.

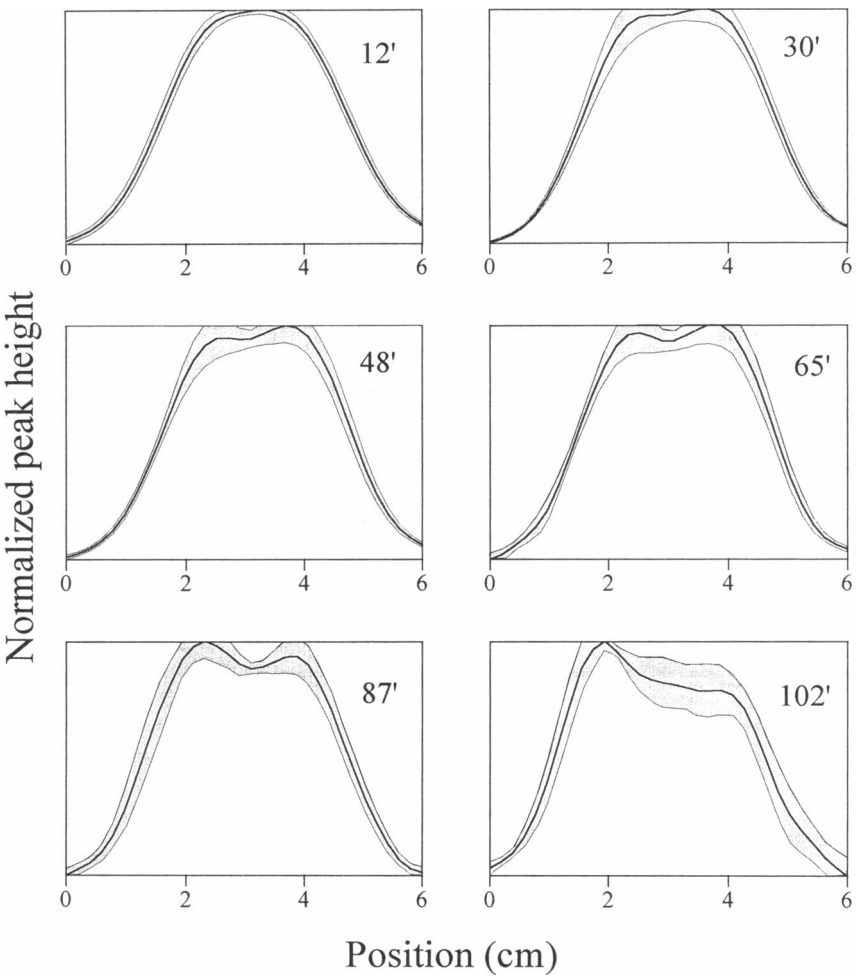


FIGURE 5 Spatial distribution obtained from the spectral spatial images by plotting the spectral peak value as a function of position. These distributions are obtained sequentially from spin label II at the mean time after IP infusion indicated in each of the six panels. The image obtained in the first distribution peaks in the middle of the animal's abdomen. The next image shows the development of a distribution peak in the region of the liver. The distinct peak in this region remains in the successive images, whereas a peak in the region of the bladder builds with time, indicative of spin probe excretion. The shaded region about a line represents the mean ± SE derived from measurements in four different animals.

In the results presented in Figs. 5 and 6, the images are presented normalized to the largest peak. On an absorption maximum, the absolute values of the spatial peaks typically diminish jointly by a factor of 4–8 over the time course presented. This is likely due to nonspecific tissue bioreduction of the free-radical nitroxyl group. The physiology and anatomy of the distribution of the spin-labeled compounds on IP injection argues against the diminution in peak height being due to bioreduction only. Solutions injected IP are absorbed by the peritoneum and the omentum, the vessels of which converge on the portal circulation feeding into the liver, which, in turn, feeds the general circulation. Blood from the general circulatory system is rapidly filtered in the kidney and excreted into the bladder. What is consistently seen in these images as noted above is the proper sequence of peak development, as one would expect from this anatomic model of distribution. The use of the normalized images (each image plotted at the same height despite the overall reduction in the number of contributing spins), therefore, eliminates or reduces the contribution of the overall bioreduction effect, allowing the technique to expose distributional or anatomic delivery patterns.

The salient result of this study is the simultaneous monitoring of the distribution of the spin label in the livers and the bladders of mice and the monitoring of their relative accumulations. We observe that the liver appears to eliminate the alcohol spin label III, through either excretion or reduction, far more rapidly than it does the carboxylate or the tertiary amine. All species appear to have a bladder accumulation, as expected for these small molecules, which are excreted in the glomerular filtrate. Whereas bioreduction undoubtedly occurs in the bladder as the result of ascorbate in the urine, the reduction of the height of the spatial peak from the bladder is, in all compounds, slower than that in the liver.

The spin labeling of drugs and the imaging of their organ compartmentalization is, perhaps, the most intriguing possibility offered by this technique. The spin labels used are covalently bound to their simple substrates, making the signal that is specific to these compounds injected. Not only do nitroxyl spin labels exhibit long half-lives in solution at neutral pH but the compounds when administered to mice over long periods of time appear to be nontoxic. Moreover, animal imaging can be accomplished in relatively short periods of time with a moderate technical upgrade, resulting in a resolution that is far better than those presented here. In summary, we believe this to be an initial example of a very useful technique to evaluate a crucial aspect of drug efficacy.

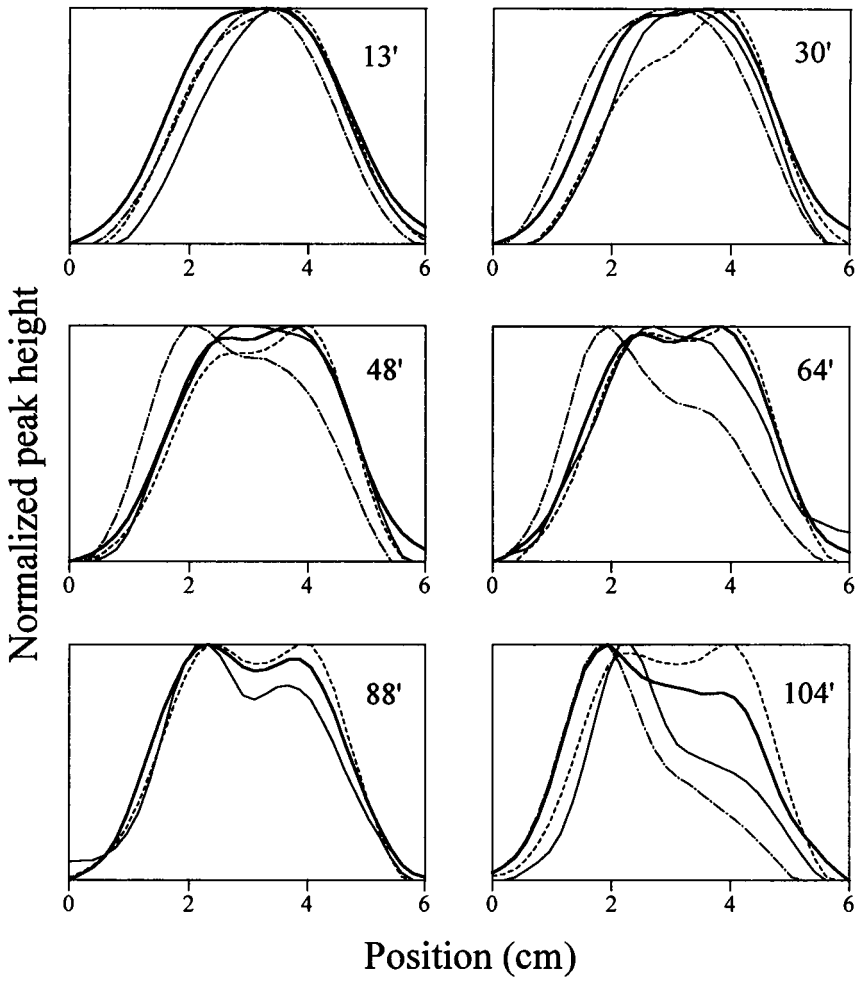


FIGURE 6 Spatial distribution from typical images of all the spin-labeled compounds I–IV described in the text (spin label I, - - -; spin label II, *thick curve*; spin label III, - • - • - • -; spin label IV, *thin curve*). The distinct patterns of the timing of the buildup of the liver and bladder peaks were readily reproducible.

This research was supported by grants from the Alcoholic Beverage Medical Research Foundation, National Insitutes of Health (CA-50679 and HL-33550). We thank Sovitj Pou for helpful suggestions and discussions concerning the preparation of several of the nitroxides and details of experimental design.

## REFERENCES

Alecci, M., A. Sotgiu, V. Ferrari, V. Quaresima, A. Sotgiu, and C. L. Ursini. 1994. Simultaneous 280 MHz EPR imaging of rat organs during nitroxide free radical clearance. *Biophys. J.* 67:1274–1279.

Antar, M. A. 1990. Radiopharmaceuticals for studying cardiac metabolism. *Int. J. Rad. Appl. Instrum. B.* 17:103–128.

Bacic, G., T. Walczak, F. Demsar, and H. M. Swartz. 1988. Electron spin resonance imaging of tissues with lipid-rich areas. *Magn. Reson. Med.* 8:209–219.

Berliner, L. J., and H. Fuji. 1985. Magnetic resonance imaging of biological specimens by electron paramagnetic resonance of nitroxide spin-labels. *Science.* 227:517–519.

Boisvert, W. E., D. Mustafi, S. Kasa, M. W. Makinen, H. J. Halpern, C. Yu, E. Barth, and M. Peric. 1993. Kinetically specific spin-label substrates of liver alcohol dehydrogenase and liver aldehyde dehydrogenase. *In* Enzymology and Molecular Biology of Carbonyl Metabolism 4. H. Weiner, D. W. Crabb, and T. G. Flynn, editors. Plenum Publishing Corp., New York.

Fuchs, J., N. Groth, T. Herrling, R. Milbradt, G. Zimmer, and L. Packer. 1992. Electron paramagnetic resonance (EPR) imaging in skin: biophysical and biochemical microscopy. *J. Invest. Dermatol.* 98:713–719.

Halpern, H. J., M. K. Bowman, D. P. Spencer, J. Van Polen, E. M. Dowey, R. J. Massoth, A. C. Nelson, and B. A. Teicher. 1989. An imaging radiofrequency electron spin resonance spectrometer with high resolution and sensitivity for in vivo measurements. *Rev. Sci. Instrum.* 60: 1040–1050.

Halpern, H. J., S. Pou, M. Peric, C. Yu, E. Barth, and G. M. Rosen. 1993. Detection and imaging of oxygen-centered free radicals with low-frequency electron paramagnetic resonance and signal-enhancing deuterium-containing spin traps. *J. Am. Chem. Soc.* 115:218–223.

Hayner, D. A., and W. K. Jenkins. 1984. The missing cone problem in computer tomography. *Comput. Vision Image Proc.* 1:83–114.

Herrling, T., N. Klimes, W. Karthe, U. Ewert, and B. Ewert. 1982. EPR zeugmatography using modulated magnetic field gradients. *J. Magn. Reson.* 49:203–211.

Hideg, K., H. O. Hankovszky, L. Lex, and G. Kulcsar. 1980. Nitroxyls: VI synthesis and reactions of 3-hydroxymethyl-2,2,5,5-tetramethyl-2,5-dihydropyrrole-1-oxyl and 3-formyl derivatives. *Synthesis.* 911–914.

Kung, H. F. 1990. Radiopharmaceuticals for CNS receptor imaging with SPECT. *Int. J. Rad. Appl. Instrum. B.* 17:85–92.

Kuppusamy, P., M. Chzhan, K. Vij, M. Shteynbuk, and J. L. Zweier. 1994. Three-dimensional spectral-spatial EPR imaging of free radicals in the heart: a technique for imaging tissue metabolism and oxygenation. *Proc. Natl. Acad. Sci. USA.* 91:3388–3392.

Lauterbur, P. C., D. N. Levin, and R. B. Marr. 1984. Theory and simulation of NMR spectroscopic imaging and field plotting by projection reconstruction involving an intrinsic frequency dimension. *J. Magn. Reson.* 59:536–541.

Liu, K. J., P. Gast, M. Moussavi, S. W. Norby, N. Vahidi, T. Walczak, M. Wu, and H. M. Swartz. 1993. Lithium phthalocyanine: a probe for

electron paramagnetic resonance oximetry in viable biological systems. *Proc. Natl. Acad. Sci. USA.* 90:5438–5442.

Loevinger, R., and M. A. Berman. 1968. Schema for absorbed-dose calculations for biologically-distributed radionuclides. Medical Internal Radiation Dose (MIRD) pamphlet No. 1. *J. Nucl. Med.* 9(1):7–14.

Loevinger, R., and M. A. Berman. 1976. Revised scheme for absorbed-dose calculations for biologically-distributed radionuclides. Medical Internal Radiation Dose (MIRD) pamphlet No. 1, revised.

Maltempo, M. M. 1986. Differentiation of spectral and spatial components in EPR imaging using 2-D image reconstruction algorithms. *J. Magn. Reson.* 69:156–161.

Maltempo, M. M., S. S. Eaton, and G. R. Eaton. 1987. Spectra-spatial two-dimensional EPR imaging. *J. Magn. Reson.* 72:449–455.

Maltempo, M. M., S. S. Eaton, and G. R. Eaton. 1988. Reconstruction of spectra-spatial two-dimensional EPR images from incomplete sets of projections without prior knowledge of the component spectra. *J. Magn. Reson.* 77:75–83.

Pou, S., P. L. Davis, G. L. Wolf, and G. M. Rosen. 1995. Use of nitroxides as NMR contrast enhancing agents for joints. *Free Rad. Res.* 23(4): 353–364.

Reba, R. C. 1993. PET and SPECT: opportunities and challenges for psychiatry. *J. Clin. Psychiatry* 54:26–32.

Rosantzev, E. G. 1970. Free Nitroxyl Radicals. Plenum Publishing Corp., New York.

Roschmann, P. 1987. Radiofrequency penetration and absorption in the human body: Limitations to high-field whole-body nuclear magnetic resonance imaging. *Med. Phys.* 14:922–931.

Stocklin, G. 1992. Tracers for metabolic imaging of brain and heart. *Eur. J. Nucl. Med.* 19:527–551.